
ENGINEERING SOFTWARE 2.0 BY INTERPOLATING NEURAL NETWORKS: UNIFYING TRAINING, SOLVING, AND CALIBRATION

Chanwook Park *

Department of Mechanical Engineering
Northwestern University
Evanston, IL 60208
chanwookpark2024@u.northwestern.edu

Sourav Saha *

Theoretical and Applied Mechanics Program
Northwestern University
Evanston, IL 60208
sourav023@u.northwestern.edu

Jiachen Guo

Theoretical and Applied Mechanics Program
Northwestern University
Evanston, IL 60208
jiachenguo2020@u.northwestern.edu

Xiaoyu Xie

Department of Mechanical Engineering
Northwestern University
Evanston, IL 60208
xiaoyuxie2020@u.northwestern.edu

Satyajit Mojumder

Theoretical and Applied Mechanics Program
Northwestern University
Evanston, IL 60208
satyajitmojumder2022@u.northwestern.edu

Miguel A. Bessa

School of Engineering
Brown University
Providence, RI
miguel_bessa@brown.edu

Dong Qian

Department of Mechanical Engineering
University of Texas at Dallas
Richardson, TX 75080
dong.qian@utdallas.edu

Wei Chen

Department of Mechanical Engineering
Northwestern University
Evanston, IL 60208
weichen@northwestern.edu

Gregory J. Wagner

Department of Mechanical Engineering
Northwestern University
Evanston, IL 60208
gregory.wagner@northwestern.edu

Jian Cao

Department of Mechanical Engineering
Northwestern University
Evanston, IL 60208
j.cao@northwestern.edu

Wing Kam Liu †

Department of Mechanical Engineering
Northwestern University
Evanston, IL 60208
w-liu@northwestern.edu

April 17, 2024

ABSTRACT

*Equal contribution with Coauthor 1 and Coauthor 2

†Corresponding author

The evolution of artificial intelligence (AI) and neural network theories has revolutionized the way software is programmed, shifting from a hard-coded series of codes to a vast neural network. However, this transition in engineering software has faced challenges such as data scarcity, multi-modality of data, low model accuracy, and slow inference. Here, we propose a new network based on interpolation theories and tensor decomposition, the interpolating neural network (INN). Instead of interpolating training data, a common notion in computer science, INN interpolates interpolation points in the physical space whose coordinates and values are trainable. It can also extrapolate if the interpolation points reside outside of the range of training data and the interpolation functions have a larger support domain. INN features orders of magnitude fewer trainable parameters, faster training, a smaller memory footprint, and higher model accuracy compared to feed-forward neural networks (FFNN) or physics-informed neural networks (PINN). INN is poised to usher in Engineering Software 2.0, a unified neural network that spans various domains of space, time, parameters, and initial/boundary conditions. This has previously been computationally prohibitive due to the exponentially growing number of trainable parameters, easily exceeding the parameter size of ChatGPT, which is over 1 trillion. INN addresses this challenge by leveraging tensor decomposition and tensor product, with adaptable network architecture.

1 Introduction

The evolution of software programming methodologies has transitioned from reliance on rigidly hard-coded instructions, governed by explicitly defined human rules, to the adoption of neural network-based algorithms. The transition is coined as "from *Software 1.0* to *Software 2.0*" [1]. The shift towards Software 2.0 has facilitated significant advancements in the domain of large language models (LLMs) and other foundational models [2, 3]. However, the application of these technologies within the field of engineering and science introduces distinct challenges. These challenges include scarcity and multi-modal aspect of data, low generalization error compared to classical numerical methods [4, 5, 6], slow inference (function evaluation) time that challenges real-time control [7, 8, 9, 10] and statistical modeling, and resource-heavy model architecture [11, 12, 13, 14].

In this article, we propose the concept of Engineering Software 2.0, which aims to advance the current generation of computational and data-driven engineering software into a new paradigm.

"Engineering Software 2.0 is an end-to-end software system that unifies training, solving, and calibration in science/engineering problems."

As one promising enabler of Engineering Software 2.0, we introduce interpolating neural networks (INN). The key ideas behind INN are: 1) discretize an input domain into non-overlapping segments whose bounds are denoted by interpolation points, 2) interpolate them with well-established interpolation techniques, and 3) optimize the values and coordinates of the interpolation points. This is distinct from the way it is referred to in the machine learning (ML) community; interpolation in ML generally refers to the interpolation of training data, which may cause overfitting. Figure 1b-d clearly shows the uniqueness and simplicity of our approach: interpolation of points (red dots in Figure 1d). Note that one can also extrapolate for a certain range if the interpolation points are located outside of the range of training data.

INN resolves the exponentially growing computational cost of high-dimensional interpolation by leveraging the separation of variables and tensor decomposition [15, 16, 17, 18] (see Figure 1e). INN facilitates three major tasks in computational science and engineering: 1) train (or learn) on both experimental and simulation data with very high accuracy and minimal memory footprint, 2) solve extremely challenging high-dimensional problems with statistics involved, and 3) calibrate (or solve inverse problems) for uncertain parameters.

Our results demonstrate that INN can markedly enhance training/inference speed and model accuracy compared to the feed-forward neural network (FFNN) or physics-informed neural network (PINN)[19] by dramatically reducing the number of trainable parameters and network connectivity. This also results in a huge reduction in the usage of random-access memory (RAM) and disk storage, facilitating the transferability of a trained/solved model across multiple workstations. Furthermore, INN can adapt its network structure to further improve model accuracy or to incorporate statistical behavior. INN has a huge potential of replacing FFNN and convolutional neural network (CNN) [20] in modern AI models with the aforementioned benefits.

2 INN: Unifying Training/Learning, Solving, and Calibration

Interpolating Neural Network (INN) is a systematically pruned neural network based on interpolation theories [17, 22] that leverage classical numerical methods such as finite element [23] and meshfree methods [24, 25]. Although these numerical methods and the neural network theory have been developed by seemingly different groups of researchers,

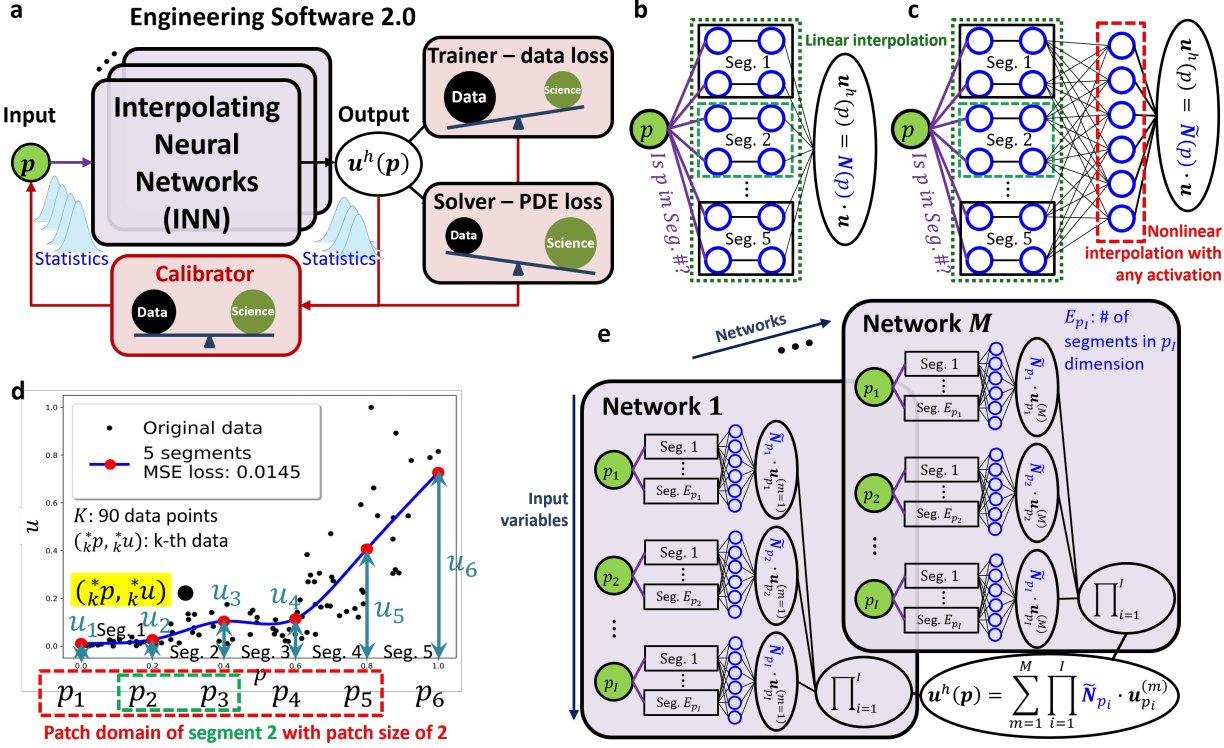


Figure 1: Overview of Interpolating Neural Networks (INN). **a**, INN forms the backbone of Engineering Software 2.0 that unifies training, solving, and calibration. The trainer employs data-driven loss functions (e.g., mean squared (MSE) error loss) while the solver adopts a residual loss of a partial differential equation (PDE). A trained/solved INN model can then be employed as a forward model of a calibrator to solve an inverse problem. It can also predict output uncertainties originating from input variables and the model itself. **b-c**, One-dimensional (1-D) input INN discretized with 5 segments and 6 interpolation points, where **c** is an expansion of segment 2. The purple lines denote a logical operation that sends an input variable p to only one segmental network (black solid boxes) that it belongs to. The first two layers (green dotted boxes) build linear interpolants and the third layer (red dotted box) builds nonlinear interpolants ($\tilde{N}(p)$). Finally, the outputs of the last hidden layer are dot-produced with corresponding point values (\mathbf{u}) to yield the interpolated output, $u^h(p)$. **d**, a regression problem [21] trained with **b-c**, highlighted for segment 2. **e**, INN for multi-dimensional (I -D) inputs. Each network ($m = 1, \dots, M$) has I different 1-D INNs illustrated in **b**, followed by a product operator $\prod_{i=1}^I$. The outputs of all networks are added to yield the interpolated output, $u^h(p)$.

they share one thing in common; the goal is to find a function. The former finds a solution field of a differential equation while the latter finds an input-output relationship. INN is built upon this similarity and it forms the backbone of Engineering Software 2.0 that unifies training, solving, and calibration, as illustrated in Figure 1a.

2.1 INN for Training

The key idea of INN is that the domain of an input variable is divided into non-overlapping segments with interpolation points, interpolation functions (or interpolants, which will be used interchangeably) are built for each segment, then the interpolation points (both values and coordinates) are optimized. An illustrative regression problem is shown in Figure 1d. Assume that the one-dimensional input domain is uniformly divided into 5 segments with 6 interpolation points whose coordinates ($p_1 \sim p_6$) are fixed for now. For a given input data $(_kp)$, we first find out which segment the input data belongs to; the input data $_kp$ is in segment 2. Then a patch domain is considered that encompasses neighboring segments, where the size is determined by *patch size*, s . Since the patch domain of segment 2 consists of five interpolation points ($u_1 \sim u_5$), five INN interpolants ($\tilde{N}_j(p)$) are constructed to nonlinearly interpolate at $p = kp$ as:

$$u^h({}^*_k p) = [\tilde{N}_1({}^*_k p) \quad \tilde{N}_2({}^*_k p) \quad \tilde{N}_3({}^*_k p) \quad \tilde{N}_4({}^*_k p) \quad \tilde{N}_5({}^*_k p)] \cdot \begin{bmatrix} u_1 \\ u_2 \\ u_3 \\ u_4 \\ u_5 \end{bmatrix}. \quad (1)$$

See Supplementary Section for detailed construction of INN interpolants.

The corresponding neural network structures are illustrated in Figure 1b-c and Figure 2a for segment 2. INN's weights and biases are functions of coordinates (p_i) and values (u_i) of the interpolation points, and INN hyper-parameters (e.g., patch size s , dilation parameter a). Assuming that the coordinates and hyper-parameters are fixed (i.e. INN interpolants are fixed), the only trainable parameters are the interpolation point values (u_j), which appear as weights between the third hidden layer and the output layer (see Figure 1c). For this reason, INN can dramatically reduce trainable parameters compared to FFNN, yielding faster training, less memory requirements, and faster inference. It is worth noting that the neural network structure of INN is not limited to Figure 1b; one can build INN with the first two hidden layers only for linear interpolation, or use other interpolation techniques such as meshfree [24, 25] or splines [26] that may result in different structures.

The goal of training for a regression problem is to minimize the distance between the prediction $u^h({}^*_k p)$ and the output data ${}^*_k u$. Thus, a mean-squared error (MSE) loss function is used:

$$\text{loss}(\mathbf{u}) = \text{loss}(u_1, u_2, \dots, u_6) = \frac{1}{K} \sum_k (u^h({}^*_k p) - {}^*_k u)^2, \quad (2)$$

where K is the number of training data. Finally, an optimization problem is formulated as:

$$\underset{\mathbf{u}}{\text{minimize}} \text{loss}(u_1, u_2, \dots, u_6). \quad (3)$$

We can also update the interpolants (i.e., the coordinates of interpolation points and INN hyper-parameters). For example, one can optimize $p_1 \sim p_6$ to optimize the positions of the interpolation points (or the length of each segment) by:

$$\underset{\mathbf{u}}{\text{minimize}} \text{loss}(p_1, \dots, p_6; u_1, \dots, u_6), \quad (4)$$

but still, the training cost is significantly lower than FFNN. One can also update the number of interpolation points adaptively, as discussed in Supplementary Information.

Similar to the activation function that determines the nonlinearity of FFNN, the *convolution patch functions*, appearing as the weights between the second and third hidden layers (\mathcal{W}) in Figure 1c, control nonlinear interpolation in INN. The formulation of convolution patch functions with arbitrary activation is schematically illustrated in Figure 2a and discussed in detail in Supplementary Section. As the activation function dictates the interpolation basis, there might be a better- or worse- performing activation function depending on the ground truth function to be trained. Two illustrative examples are provided in Figure 2c,e. In general, activation functions close to the ground truth function yield low errors. Especially in Figure 2d where the two are the same, INN can reach a perfect fit to the ground truth function. Thus, activation functions are tunable hyperparameters. One can adaptively optimize them for each segment during training, which is prohibitive or less common in most neural networks [27, 28] (see Supplementary Section for detailed demonstration).

The INN interpolants can also be formulated for multi-dimensional inputs. In references [17, 22], which are the predecessors of INN theory, the benefits of those interpolants for solving 2D and 3D partial differential equations (PDEs) are demonstrated. However, the computational cost of building multi-dimensional interpolants grows exponentially with the input dimension. To tackle this problem, we propose a projected interpolation to INN, mathematically inspired by the separation of variables, proper orthogonal decomposition [29], proper generalized decomposition [30], and tensor decomposition [15].

The projected interpolation converts n -dimensional interpolation into " n " 1-dimensional interpolations with " M " different modes. With it, one can dramatically (typically by orders of magnitude) reduce the degrees of freedom (DoFs) of high-dimensional problems. Consider an I -input and L -output system. Similar to the single-input case, we discretize each input dimension and find the values of interpolation points through optimization. The predicted value at k -th input data ${}^*_k p$ using INN becomes:

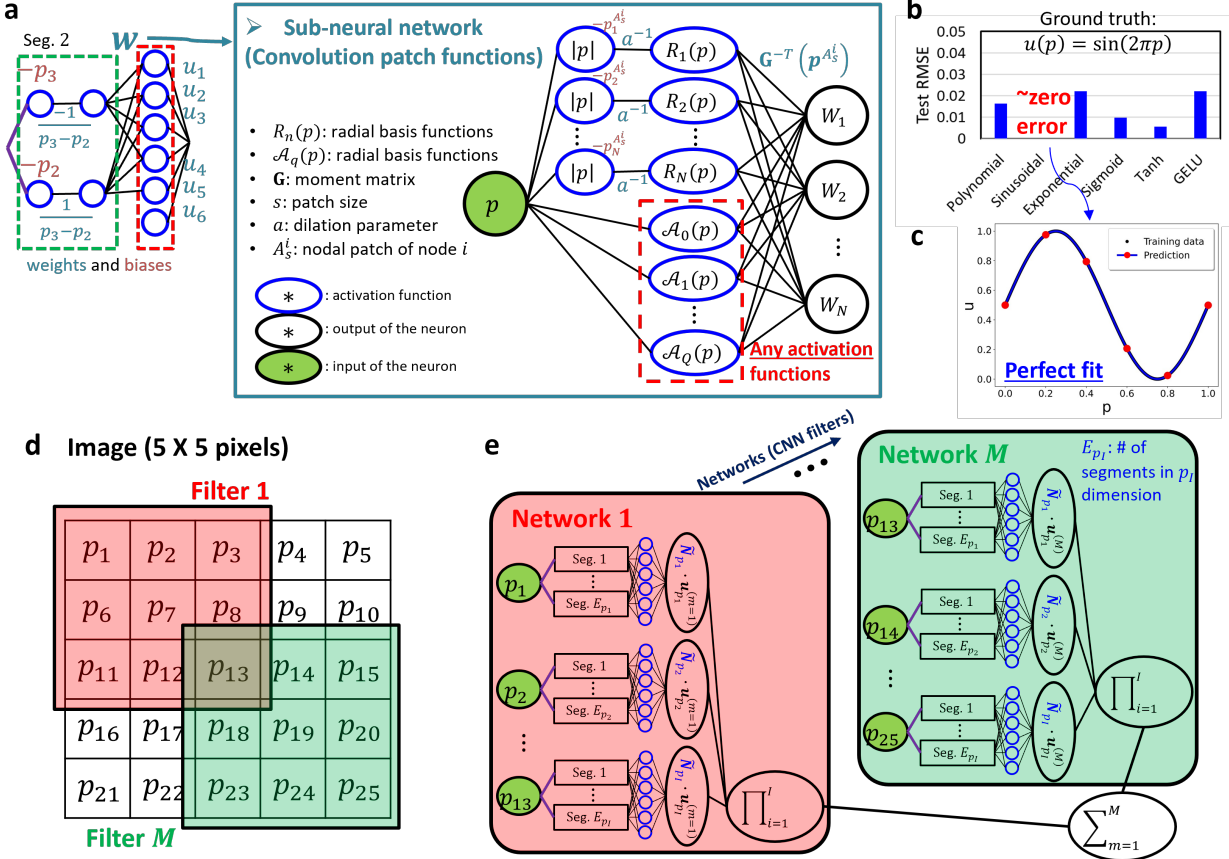


Figure 2: **a**, A sub-neural network that constructs convolution patch functions (weights between the second and third hidden layers, \mathcal{W}). Weights and biases in this network are functions of coordinates of interpolation points (p_i) and INN hyper-parameters. See supplementary Information for detailed formulation. **b-c**, Effect of activation functions when a sinusoidal ground truth function is trained. Details can be found in Supplementary Information. **c**, A trained INN with sinusoidal activation function showing a perfect fit to the ground truth function. **d-e**, convolutional neural network (CNN) version of INN where each network corresponds to a CNN filter.

$$\begin{aligned} \mathbf{u}^h({}^k\mathbf{p}) &= \mathbf{u}^h({}^k p_1, {}^k p_2, \dots, {}^k p_I) = \sum_{m=1}^M [\tilde{\mathbf{N}}_{p_1}({}^k p_1) \cdot \mathbf{u}_{p_1}^{(m)}] \odot [\tilde{\mathbf{N}}_{p_2}({}^k p_2) \cdot \mathbf{u}_{p_2}^{(m)}] \odot \dots \odot [\tilde{\mathbf{N}}_{p_I}({}^k p_I) \cdot \mathbf{u}_{p_I}^{(m)}] \\ &= \sum_{m=1}^M \prod_{i=1}^I [\tilde{\mathbf{N}}_{p_i}({}^k p_i) \cdot \mathbf{u}_{p_i}^{(m)}] \end{aligned} \quad (5)$$

where ${}^k\mathbf{p} = [{}^k p_1, {}^k p_2, \dots, {}^k p_I]$ is the input variables of k -th training data, \mathbf{u}^h is the corresponding interpolated output vector of length L , M is the number of modes (or networks; we use them interchangeably in INN), $\tilde{\mathbf{N}}_{p_i}(\cdot)$ and $\mathbf{u}_{p_i}^{(m)}$ are the one-dimensional INN interpolants and values of interpolation points for the input dimension p_i , respectively, and \odot refers to the component-wise multiplication of the same dimension. Starting from Eq. 5, p_i will denote i -th input variable or dimension, and $p_{i,j}$ will refer to the j -th coordinate in i -th input dimension. If all input dimensions are discretized with the same number of segments (or interpolation points, denoted as J), the values of mode 1 through mode M become a 4-th order tensor of size (M, I, J, L) , which is the trainable parameters of INN. See Supplementary Section for detailed training algorithms.

The neural network structure of the multi-dimensional INN is illustrated in Figure 1c. Each mode in Eq. 5 is represented by an independent neural network with three hidden layers. Each network has the potential to possess unique hyperparameters, including the number of segments and activation function, thereby creating a new realm of

significant versatility. For instance, one can start with a high number of segments for earlier networks and gradually reduce the level of discretization for later networks, mimicking multi-resolution filtering in wavelet analysis or Fourier transform [31], which has not been realized in previous works [17, 18].

It is also possible to nullify some input variables mode by mode, which is similar to the concept of random dropout in neural networks [32] or the convolutional neural networks (CNN) [20]. The method is simple: set interpolation point values of an input variable p_i as 1, $u_{p_i}^{(m)} = 1$, like applying Dirichlet boundary conditions for solving partial differential equations. As the interpolation of network (m) is a product of "I" one-dimensional interpolations, this will result in dropping out or nullifying these inputs. One special case of manual dropout resembling CNN is illustrated in Figure 3d-e. Given a 5×5 pixels image, instead of having the entire 25 pixels as input variables, one can construct each network such that it takes inputs of one CNN filter. When a 3×3 filter is used with a stride of 1, each INN network gets 9-pixel inputs and the total number of networks becomes $M = 9$. We conducted benchmarks on the fashion-MNIST dataset [33] with this idea which will be discussed in the following section.

2.2 INN for solving

The INN solver uses the same neural network structure as the trainer but is equipped with a loss function formulated from an equation to be solved. Here, we introduce a general formulation for solving parameterized time-dependent partial differential equations (PDEs), which is prohibitive for most numerical methods and machine learning approaches [34]. We construct an optimization problem from the PDE, which has been introduced as the residual minimization strategy [35] or the Petrov-Galerkin loss function [36, 37].

The approximate solution field of INN for a space (\mathbf{x}) - time (t) - parameter ($\boldsymbol{\theta}$) problem is given as:

$$\mathbf{u}^h(\mathbf{x}, t, \boldsymbol{\theta}) = \sum_{m=1}^M [\tilde{\mathbf{N}}_{x_1}(x_1) \cdot \mathbf{u}_{x_1}^{(m)}] \odot \dots \odot [\tilde{\mathbf{N}}_{x_d}(x_d) \cdot \mathbf{u}_{x_d}^{(m)}] \odot [\tilde{\mathbf{N}}_t(t) \cdot \mathbf{u}_t^{(m)}] \odot [\tilde{\mathbf{N}}_{\theta_1}(\theta_1) \cdot \mathbf{u}_{\theta_1}^{(m)}] \odot \dots \odot [\tilde{\mathbf{N}}_{\theta_k}(\theta_k) \cdot \mathbf{u}_{\theta_k}^{(m)}]. \quad (6)$$

where d and k are the spatial dimension and the number of parameters, respectively. Similar to the trainer, the goal is to find values of interpolation points: $\mathbf{u}_{\mathbf{x}}^{(1 \sim M)}, \mathbf{u}_t^{(1 \sim M)}, \mathbf{u}_{\boldsymbol{\theta}}^{(1 \sim M)}$. The loss function is derived from weighted integrals of the differential equation ($loss^{PDE}$) and boundary ($loss^{BC}$)/initial ($loss^{IC}$) conditions:

$$loss = loss^{PDE} + \tau_{BC} \cdot loss^{BC} + \tau_{IC} \cdot loss^{IC} \quad (7)$$

See Supplementary Section for detailed derivations of the loss function, test function, and numerical integration. The weights τ_{BC} and τ_{IC} control the rate of convergence and can be user-specified.

2.3 INN for calibration

The word calibration in mathematics refers to a reverse process of regression, where a known or measured observation of the output variables ($^* \mathbf{u}$) is used to predict the corresponding input variables ($^* \mathbf{p}$). By definition, it is similar to solving an inverse problem in Engineering. To build a good calibrator, having an accurate forward model is of paramount importance, followed by building a good optimizer for the inverse problem. A trained or solved INN has the potential to be a superior candidate for the forward model inside a calibrator. It is fully differentiable and accurate, equipped with fast inference time (\sim milliseconds). A general formulation of the INN calibrator is described below:

$$^* \mathbf{p} = \underset{\mathbf{p}}{\operatorname{argmin}} \frac{1}{K} \sum_k (\mathbf{u}^h(\mathbf{p}) - {}_k \mathbf{u})^2, \quad (8)$$

where $\mathbf{u}^h(\mathbf{p})$ is the trained or solved forward model, ${}_k \mathbf{u}$ is the k -th measured observation and $^* \mathbf{p}$ is the calibrated input variables.

3 Benchmark Demonstration

To demonstrate the advantages of INN for training, calibration, and solving, we present several benchmarks for each subject. The benchmark problems include training of data that follow scientific equations, classification of spiral data,

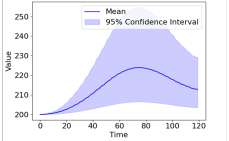
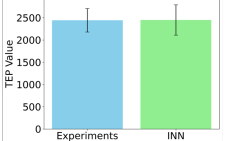
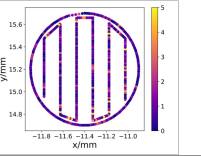
Category	Description	Input/output	Results	
			Visualization	Remarks
Solving	High-dimensional governing equation for L-PBF $\frac{\partial T(\mathbf{x}, t)}{\partial t} - k\Delta T(\mathbf{x}, t) = S_h(\mathbf{x}, y, P, \eta, R, d)$	Space-time-parameter inputs (9)/Thermal field		<ul style="list-style-type: none"> $10^3 - 10^5$ times faster solver compared to FEM and PINN. $10^5 - 10^6$ times less storage requirement compared to FEM and PINN.
Calibration	Heat source parameter calibration $Q^{in}(\mathbf{x}, t, \mathbf{p}) = \frac{2\mathcal{P}\eta}{\pi r_b^2 d} e^{-\frac{2(x^2+y^2)}{r_b^2}}$	Depth, $d = p_1 \frac{\mathcal{P}}{V}$ Absorptivity, $\eta = p_2 \frac{\mathcal{P}}{V}$ Laser beam radius, $r_b = p_3 \frac{\mathcal{P}}{V}$		<ul style="list-style-type: none"> Only requires 7 simulations for 3 parameters Calibration accuracy = 6.7%
Training	Real-time online monitoring of L-PBF process	21 Mechanistic features, thermal field, current laser power (input)/laser power required for the next layer		<ul style="list-style-type: none"> 18 to 31 times faster training than FFNN. Requires 82% less trainable parameters than FFNN. More accurate prediction than FFNN.

Figure 3: Application of the INN methods to scientific and engineering problems. During solving a very high-dimensional manufacturing process of L-PBF, the INN method is 10^5 and 10^6 times faster than FEM and PINN. For heat source calibration, INN requires very high-fidelity data to develop an accurate surrogate model. To develop a data-driven real-time online monitoring tool, INN uses only 18% training parameters and is 18-31 times faster compared to FFNN.

classification of the fashion-MNIST dataset [33], calibration of parameters in the scientific equations and electrode manufacturing data [38], and solving of a parameterized partial differential equation (PDE). Except for the fashion-MNIST classification, all benchmark demonstrations are provided in the supplementary information, clearly revealing significant benefits such as less trainable parameters, high accuracy, less memory requirement, fast training, and inference time. One can also find how the INN hyperparameters are selected in Supplementary Information.

Table 1 shows the benchmark result of the fashion-MNIST image classification problem [33]. Results of the support vector classifier (SVC), random forest classifier (RFC), and tensor neural network (TNN) are taken from references, while FFNN, INN, and INN (CNN type) are from our own source code. Compared to well-established classifiers (SVC, RFC, FFNN), INNs can achieve comparable high accuracy with fewer trainable parameters. Especially, the CNN-type INN can only use around 50% parameters of FFNN without significantly sacrificing the prediction accuracy. It is worth noting that the TNN, which shares a similar mathematical background with INN (i.e., tensor decomposition and contraction), is less accurate than all the others and limited to smaller image size [39].

Table 1: Benchmark result of the fashion-MNIST classification.

	Support Vector Classifier [33]	Random Forest Classifier [33]	Tensor Neural Network [39]	FFNN	INN	INN (CNN type)
Features	RBF kernel Gamma: 10	Estimators: 100 Max depth: 100	Reduced image 8 × 8 pixels	[784, 512, 256, 10] neurons	30 networks 1 segments	5 × 5 filter stride: 1
Test accuracy	0.8970	0.8730	0.8343	0.8918	0.8813	0.8731

4 Scientific and Engineering applications

This section will illustrate how Engineering Software 2.0 can be applied to model various facets of metal additive manufacturing by integrating training, solving, and calibration processes. Laser Powder-bed Fusion (L-PBF) is a type of metal additive manufacturing in which metal powders are layered and melted by a laser beam to create objects that match the provided CAD designs [40]. The added flexibility of L-PBF comes with very large design space and spatially varying microstructure after manufacturing. Therefore, considerable research is being devoted to employing

in situ monitoring data for real-time control of L-PBF processes to minimize variability [7]. The modeling aspect of L-PBF spans across modeling the manufacturing process with very high design space (solving), computing the internal relationship among different parameters of manufacturing (calibrating), and designing an online monitoring and control system for L-PBF (training).

The governing equation for modeling the manufacturing processing is given by

$$\frac{\partial T(\mathbf{x}, t)}{\partial t} - k\Delta T(\mathbf{x}, t) = Q_h(x, y, t, P, R, \eta, d) \quad (9)$$

This is a heat conduction equation where the moving laser heat source is incorporated through the source term, Q_h . The equation involves spatial parameter (x, y, z) , temporal variable t , thermal conductivity k , power P , beam radius R , absorptivity η , and laser depth d . For the simplest case of single track laser pass, the initial condition is $T(\mathbf{x}, 0) = 0$, and the boundary conditions are $T = \tilde{T}$ in $\partial\Omega_T$, and $\frac{\partial T}{\partial \mathbf{x}} \cdot \mathbf{n} = \bar{q}$ in $\partial\Omega_q$.

4.1 Solving High Dimensional Space-Time-Parameter Heat Equation

Equation 9 has 9 input variables; 3 for spatial domain, 1 for time domain, and 5 for parametric domain. See, Supplementary Section for a detailed problem definition. This equation is prohibitive for process design with most existing computational methods, including finite element method (FEM)-based data-driven method and physics informed neural network (PINN) [19].

To solve the problem with FEM-based data-driven method, one first needs to sample from the 5-dimensional parametric domain, followed by running space-time FEM for each sampled parameter set. Then the FEM solution should be stored as training data, and a neural network surrogate model will be trained based on the data. The computational cost required is prohibitive as illustrated in Supplementary Section. Moreover, as a larger number of training data are generated due to the high dimensionality of the input domain, this method becomes prohibitive in terms of data storage. Running large-scale FEM simulation is also memory inefficient.

PINN is a unified framework of training and solving such parameterized PDEs, however, the computational cost still grows exponentially as the number of input variables grows. As illustrated in Supplementary Section, it is almost impossible to solve this 9-dimensional equation. In addition, the convergence of solution accuracy is not guaranteed, making it skeptical if PINN can even find a good solution for more than 7 input variables. PINN also suffers from memory issues for GPU training due to the exponential growth of the collocation points (although batch training can be adopted to alleviate memory usage).

Contrary to FEM and PINN, INN solves this space-time-parameter problem all at once. As it is based on the projected interpolation, the trainable parameters linearly grow with the input variables, making the computational cost manageable. Meanwhile, since tensor-decomposed data structures are leveraged, INN has the benefits of significant memory efficiency and storage gain especially for high-dimensional problems. A detailed comparison is provided in Supplementary Section.

On another note, once the parametric solution of the AM problem is obtained, we can easily investigate uncertainty propagation by imposing probabilistic distributions on the inputs of INN, thanks to the tensor-decomposed data structure. Figure 3 shows the uncertainty of the output when the inputs are assumed as independent Gaussian variables (see details in Supplementary Section).

4.2 Calibration of Heat Source Parameters for Additive Manufacturing

In this example, the INN is used for calibrating a model of heat source of L-PBF. Usually, a Gaussian beam profile is assumed as a volumetric heat source in L-PBF modeling [41]. The heat source equation reads,

$$Q_h(\mathbf{x}, t, \mathbf{p}) = \frac{2\mathcal{P}\eta}{\pi r_b^2 d} e^{-\frac{2(x^2+y^2)}{r_b^2}} \quad (10)$$

where, $z_{top} - z \leq d$. The notations follow Eq. 9. To get an accurate solution, some parameters need to be calibrated against experimental data. For example, three calibration parameters p_1 , p_2 , and p_3 can be defined as, $d = p_1 \frac{\mathcal{P}}{V}$, $\eta = p_2 \frac{\mathcal{P}}{V}$, and $r_b = p_3 \frac{\mathcal{P}}{V}$. Here, V is the scan speed. However, the challenges for calibrating these parameters are: 1) the computational models are often very expensive to perform even one forward run, 2) the computational models are not automatic differentiable, and 3) limited calibration data is available. As a demonstration for this problem, INN

is trained for 7 sets of melt pool temperature data generated by FEM. Later, this trained INN is used for optimizing the three aforementioned parameters using gradient-based optimizers. Even with only 7 sets of simulation data, the INN model could generate calibrated parameters that produce melt pool temperature (or TEP) within 6.4% of the experimental data (see Figure 3).

4.3 Real-time Online Control of Laser Powder Bed Fusion Additive Manufacturing

In this application, the interpolating neural network is used to devise an online control system for L-PBF additive manufacturing. The goal is to maintain a homogeneous melt pool temperature. The hypothesis is *a homogeneous melt pool temperature across each layer of material deposition will reduce the variability in the microstructure and mechanical properties*. The fundamental challenge of implementing a model predictive control system for such a system is the computational time required for the forward prediction (involving finite element or computational fluid dynamics models), and the lack of automatic differentiation capabilities in the available computational models. The contemporary data-driven models require a significant amount of data and training parameters for accurate prediction which in turn limit the applicability of these methods for real-time prediction. Therefore, a fast, memory-efficient, and differentiable computational method is required.

For prediction, the data is generated by fusing experiments and computational methods (see Supplementary Section for details). The online control loop uses the INN model to inform the manufacturing machine. There are two models: a) *the forward model* uses the mechanistic features (precomputed based on the tool path and geometry of the build to generalize a data-driven model for unseen tool path and geometric features; more details can be found in [42]), and melt pool temperature of the previous layer (measured by the sensor as Thermal Emission Plank (TEP) signal; more details in the supplementary information) to predict the TEP/melt pool temperature in the next layer for an uncontrolled process. The uncontrolled TEP is converted to a homogenized TEP over the entire layer. b) *the inverse model* takes this targeted, homogenized TEP as the input along with the previous layer's mechanistic features to predict the required laser power for the next layer. The laser power is then exported to the machine to print the next layer. The forward model is trained on experimentally observed data while the inverse model is trained on computational data coming from a finite element solver. The INN model is applied for both forward and inverse prediction and compared against FFNN. Figure 3 shows that for the inverse model INN is at least 18 to 31 times faster to train compared to the FFNN to reach the same level of training error, and it uses only about 18% of the parameters that FFNN uses. The speed-up depends on the amount of data used. The INN method is consistently more accurate compared to FFNN (see Supplementary Section for more details).

5 Conclusions

We show that interpolating neural networks (INN) can train, solve, and calibrate scientific and engineering problems that are extremely challenging or prohibitive for existing numerical methods or machine learning models. The keys to INN's success in those problems are 1) it interpolates virtual points with well-established interpolation theories (not interpolating training data with a black-box network) and 2) it leverages the idea of separation of variables and tensor decomposition to resolve the curse of dimensionality. Due to the significantly reduced trainable parameters without losing approximation capabilities, INN can train faster with less memory requirement, and achieve extremely high model accuracy and fast inference time.

As this is the original article on INN, we have myriads of research questions that may gather huge research interests across various areas including but not limited to scientific machine learning, applied mathematics, computer vision, and data science. To mention a few:

- Multi-resolution aspect (i.e., a varying number of segments across INN networks, M) of INN needs to be investigated.
- Convergence of INN for training can be proved mathematically.
- Theoretical studies on the generalization of INN as a graph neural network (GNN) are needed.
- INN training on ensembles of training data might be a way to enhance the generality of the model for image problems or noisy data.

We expect INN can open a next-generation Engineering Software 2.0 that not only merges separate modules of training, solving, and calibration but also tackles extremely challenging problems in the science and engineering domain.

References

- [1] A. Karpathy, Software 2.0 (Mar 2017).
URL <https://karpathy.medium.com/software-2-0-a64152b37c35>
- [2] M. Moor, O. Banerjee, Z. S. H. Abad, H. M. Krumholz, J. Leskovec, E. J. Topol, P. Rajpurkar, Foundation models for generalist medical artificial intelligence, *Nature* 616 (7956) (2023) 259–265.
- [3] A. Vaswani, N. Shazeer, N. Parmar, J. Uszkoreit, L. Jones, A. N. Gomez, Ł. Kaiser, I. Polosukhin, Attention is all you need, *Advances in neural information processing systems* 30 (2017).
- [4] L. Lu, P. Jin, G. Pang, Z. Zhang, G. E. Karniadakis, Learning nonlinear operators via deepnet based on the universal approximation theorem of operators, *Nature machine intelligence* 3 (3) (2021) 218–229.
- [5] C. Zhang, A. Shafeezadeh, Simulation-free reliability analysis with active learning and physics-informed neural network, *Reliability Engineering & System Safety* 226 (2022) 108716.
- [6] S. Goswami, K. Kontolati, M. D. Shields, G. E. Karniadakis, Deep transfer operator learning for partial differential equations under conditional shift, *Nature Machine Intelligence* 4 (12) (2022) 1155–1164.
- [7] Y. Cai, J. Xiong, H. Chen, G. Zhang, A review of in-situ monitoring and process control system in metal-based laser additive manufacturing, *Journal of Manufacturing Systems* 70 (2023) 309–326.
- [8] G. Leopold, Aws to offer nvidia's t4 gpus for ai inferencing (Mar 2019).
URL <https://www.hpcwire.com/2019/03/19/aws-upgrades-its-gpu-backed-ai-inference-platform/>
- [9] J. Barr, Amazon ec2 update – inf1 instances with aws inferentia chips for high performance cost-effective inferencing (Dec 2019).
URL <https://aws.amazon.com/blogs/aws/amazon-ec2-update-inf1-instances-with-aws-inferentia-chips-for/>
- [10] A. Brohan, N. Brown, J. Carbajal, Y. Chebotar, J. Dabis, C. Finn, K. Gopalakrishnan, K. Hausman, A. Herzog, J. Hsu, et al., Rt-1: Robotics transformer for real-world control at scale, *arXiv preprint arXiv:2212.06817* (2022).
- [11] S. Dhar, J. Guo, J. Liu, S. Tripathi, U. Kurup, M. Shah, A survey of on-device machine learning: An algorithms and learning theory perspective, *ACM Transactions on Internet of Things* 2 (3) (2021) 1–49.
- [12] E. Li, L. Zeng, Z. Zhou, X. Chen, Edge ai: On-demand accelerating deep neural network inference via edge computing, *IEEE Transactions on Wireless Communications* 19 (1) (2019) 447–457.
- [13] L. G. Wright, T. Onodera, M. M. Stein, T. Wang, D. T. Schachter, Z. Hu, P. L. McMahon, Deep physical neural networks trained with backpropagation, *Nature* 601 (7894) (2022) 549–555.
- [14] A. Momeni, B. Rahmani, M. Malléjac, P. Del Hougne, R. Fleury, Backpropagation-free training of deep physical neural networks, *Science* 382 (6676) (2023) 1297–1303.
- [15] T. G. Kolda, B. W. Bader, Tensor decompositions and applications, *SIAM review* 51 (3) (2009) 455–500.
- [16] L. Zhang, Y. Lu, S. Tang, W. K. Liu, Hidenn-td: Reduced-order hierarchical deep learning neural networks, *Computer Methods in Applied Mechanics and Engineering* 389 (2022) 114414.
- [17] Y. Lu, H. Li, L. Zhang, C. Park, S. Mojumder, S. Knapik, Z. Sang, S. Tang, D. W. Apley, G. J. Wagner, et al., Convolution hierarchical deep-learning neural networks (c-hidenn): finite elements, isogeometric analysis, tensor decomposition, and beyond, *Computational Mechanics* (2023) 1–30.
- [18] H. Li, S. Knapik, Y. Li, C. Park, J. Guo, S. Mojumder, Y. Lu, W. Chen, D. W. Apley, W. K. Liu, Convolution hierarchical deep-learning neural network tensor decomposition (c-hidenn-td) for high-resolution topology optimization, *Computational Mechanics* (2023) 1–20.
- [19] M. Raissi, P. Perdikaris, G. E. Karniadakis, Physics-informed neural networks: A deep learning framework for solving forward and inverse problems involving nonlinear partial differential equations, *Journal of Computational Physics* 378 (2019) 686–707.
- [20] Y. LeCun, Y. Bengio, et al., Convolutional networks for images, speech, and time series, *The handbook of brain theory and neural networks* 3361 (10) (1995) 1995.
- [21] W. K. Liu, Z. Gan, M. Fleming, Mechanistic data science for STEM education and applications, Springer, 2021.
- [22] C. Park, Y. Lu, S. Saha, T. Xue, J. Guo, S. Mojumder, D. W. Apley, G. J. Wagner, W. K. Liu, Convolution hierarchical deep-learning neural network (c-hidenn) with graphics processing unit (gpu) acceleration, *Computational Mechanics* (2023) 1–27.
- [23] W. K. Liu, S. Li, H. S. Park, Eighty years of the finite element method: Birth, evolution, and future, *Archives of Computational Methods in Engineering* 29 (6) (2022) 4431–4453.

- [24] W. K. Liu, S. Jun, Y. F. Zhang, Reproducing kernel particle methods, *International journal for numerical methods in fluids* 20 (8-9) (1995) 1081–1106.
- [25] W. K. Liu, S. Jun, S. Li, J. Ade, T. Belytschko, Reproducing kernel particle methods for structural dynamics, *International Journal for Numerical Methods in Engineering* 38 (10) (1995) 1655–1679.
- [26] T. J. Hughes, J. A. Cottrell, Y. Bazilevs, Isogeometric analysis: Cad, finite elements, nurbs, exact geometry and mesh refinement, *Computer methods in applied mechanics and engineering* 194 (39-41) (2005) 4135–4195.
- [27] F. Agostinelli, M. Hoffman, P. Sadowski, P. Baldi, Learning activation functions to improve deep neural networks, *arXiv preprint arXiv:1412.6830* (2014).
- [28] K. He, X. Zhang, S. Ren, J. Sun, Delving deep into rectifiers: Surpassing human-level performance on imagenet classification, in: *Proceedings of the IEEE international conference on computer vision*, 2015, pp. 1026–1034.
- [29] A. Chatterjee, An introduction to the proper orthogonal decomposition, *Current science* (2000) 808–817.
- [30] A. Ammar, B. Mokdad, F. Chinesta, R. Keunings, A new family of solvers for some classes of multidimensional partial differential equations encountered in kinetic theory modeling of complex fluids, *Journal of non-Newtonian fluid Mechanics* 139 (3) (2006) 153–176.
- [31] W. K. Liu, Y. Chen, C. Chang, T. Belytschko, Advances in multiple scale kernel particle methods, *Computational mechanics* 18 (2) (1996) 73–111.
- [32] P. Baldi, P. J. Sadowski, Understanding dropout, *Advances in neural information processing systems* 26 (2013).
- [33] H. Xiao, K. Rasul, R. Vollgraf, Fashion-mnist: a novel image dataset for benchmarking machine learning algorithms, *arXiv preprint arXiv:1708.07747* (2017).
- [34] F. Chinesta, P. Ladeveze, E. Cueto, A short review on model order reduction based on proper generalized decomposition, *Archives of Computational Methods in Engineering* 18 (4) (2011) 395–404.
- [35] E. Pruliere, F. Chinesta, A. Ammar, On the deterministic solution of multidimensional parametric models using the proper generalized decomposition, *Mathematics and Computers in Simulation* 81 (4) (2010) 791–810.
- [36] E. Kharazmi, Z. Zhang, G. E. Karniadakis, Variational physics-informed neural networks for solving partial differential equations, *arXiv preprint arXiv:1912.00873* (2019).
- [37] E. Kharazmi, Z. Zhang, G. E. Karniadakis, hp-vpinns: Variational physics-informed neural networks with domain decomposition, *Computer Methods in Applied Mechanics and Engineering* 374 (2021) 113547.
- [38] R. P. Cunha, T. Lombardo, E. N. Primo, A. A. Franco, Artificial intelligence investigation of nmc cathode manufacturing parameters interdependencies, *Batteries & Supercaps* 3 (1) (2020) 60–67.
- [39] I. Convay, K. B. Whaley, Interaction decompositions for tensor network regression, *Machine Learning: Science and Technology* 3 (4) (2022) 045027.
- [40] V. Bhavar, P. Kattire, V. Patil, S. Khot, K. Gujar, R. Singh, A review on powder bed fusion technology of metal additive manufacturing, *Additive manufacturing handbook* (2017) 251–253.
- [41] Y. Li, S. Mojumder, Y. Lu, A. A. Amin, J. Guo, X. Xie, W. Chen, G. J. Wagner, J. Cao, W. K. Liu, Statistical parameterized physics-based machine learning digital twin models for laser powder bed fusion process, *arXiv preprint arXiv:2311.07821* (2023).
- [42] D. Kozjek, F. M. Carter III, C. Porter, J.-E. Mogonye, K. Ehmann, J. Cao, Data-driven prediction of next-layer melt pool temperatures in laser powder bed fusion based on co-axial high-resolution planck thermometry measurements, *Journal of Manufacturing Processes* 79 (2022) 81–90.